AFRL-RB-WP-TP-2011-3106

DYNAMICS AND CONTROL OF A MINIMALLY ACTUATED BIOMIMETIC VEHICLE: PART II - CONTROL (POSTPRINT)

David B. Doman, Michael W. Oppenheimer, and David O. Sigthorsson

Control Design and Analysis Branch
Control Sciences Division

AUGUST 2009

STINFO COPY

AIR FORCE RESEARCH LABORATORY
AIR VEHICLES DIRECTORATE
WRIGHT-PATTERSON AIR FORCE BASE, OH 45433-7542
AIR FORCE MATERIEL COMMAND
UNITED STATES AIR FORCE

REPORT DOCUMENTATION PAGE

1. REPORT DATE *(DD-MM-YY)*	2. REPORT TYPE	3. DATES COVERED *(From - To)*
August 2009	Conference Paper Postprint	05 November 2008 – 13 August 2009

4. TITLE AND SUBTITLE	5a. CONTRACT NUMBER
DYNAMICS AND CONTROL OF A MINIMALLY ACTUATED BIOMIMETIC VEHICLE: PART II - CONTROL (POSTPRINT)	In-house
	5b. GRANT NUMBER
	5c. PROGRAM ELEMENT NUMBER 62201F

6. AUTHOR(S)	5d. PROJECT NUMBER
David B. Doman, Michael W. Oppenheimer, and David O. Sigthorsson (AFRL/RBCA)	2401
	5e. TASK NUMBER N/A
	5f. WORK UNIT NUMBER Q12K

7. PERFORMING ORGANIZATION NAME(S) AND ADDRESS(ES)	8. PERFORMING ORGANIZATION REPORT NUMBER
Control Design and Analysis Branch (AFRL/RBCA) Control Sciences Division Air Force Research Laboratory, Air Vehicles Directorate Wright-Patterson Air Force Base, OH 45433-7542 Air Force Materiel Command, United States Air Force	AFRL-RB-WP-TP-2011-3106

9. SPONSORING/MONITORING AGENCY NAME(S) AND ADDRESS(ES)	10. SPONSORING/MONITORING AGENCY ACRONYM(S)
Air Force Research Laboratory Air Vehicles Directorate Wright-Patterson Air Force Base, OH 45433-7742 Air Force Materiel Command United States Air Force	AFRL/RBSD
	11. SPONSORING/MONITORING AGENCY REPORT NUMBER(S) AFRL-RB-WP-TP-2011-3106

12. DISTRIBUTION/AVAILABILITY STATEMENT
Approved for public release; distribution unlimited.

13. SUPPLEMENTARY NOTES
PAO Case Number: 88ABW-2009-3585; Clearance Date: 10 Aug 2009. Document contains color.

Conference paper published in the proceedings of the AIAA Guidance, Navigation, and Control Conference held 10 - 13 August 2009 in Chicago, IL.

14. ABSTRACT

A control strategy is proposed for a minimally-actuated flapping-wing micro air-vehicle (FWMAV). The proposed vehicle is similar to the Harvard RoboFly that accomplished the first takeoff of an insect scale flapping wing aircraft, except that it is equipped with independently actuated wings and the vehicle center-of-gravity can be manipulated for control purposes. Using the results from the derivation of the aerodynamic forces and moments from Part I, a control allocation strategy and a feedback control law are designed that enables the vehicle to achieve untethered, stabilized flight about a hover condition. The control laws are designed to make use of three actuators, two of which control the angular position of the wing in the stroke plane, and one that moves a bob-weight that manipulates the vehicle center-of-gravity. The Split-Cycle Constant-Period Frequency Modulation technique, introduced in Part I, is used to allow each wing to generate nonzero cycle-averaged rolling and yawing moments. The technique achieves this objective by varying the frequency of the oscillators, that drive each wing throughout the wing-beat cycles, such that the dynamic pressure acting on each wing during the upstroke is different from that which acts on the wing during the downstroke. Pitching moment and high speed translation are controlled by varying the vehicle center-of-gravity using a bob-weight actuator.

15. SUBJECT TERMS
flapping wing micro air vehicles, MAV, flight control, minimal actuation

16. SECURITY CLASSIFICATION OF:			17. LIMITATION OF ABSTRACT:	18. NUMBER OF PAGES	19a. NAME OF RESPONSIBLE PERSON (Monitor)
a. REPORT	**b. ABSTRACT**	**c. THIS PAGE**	SAR	30	1Lt Zachary H. Goff
Unclassified	Unclassified	Unclassified			**19b. TELEPHONE NUMBER** *(Include Area Code)* N/A

Dynamics and Control of a Minimally Actuated Biomimetic Vehicle:

Part II - Control

Michael W. Oppenheimer [*]

David B. Doman [†]

David O. Sigthorsson [‡]

A control strategy is proposed for a minimally-actuated flapping-wing micro air-vehicle (FWMAV). The proposed vehicle is similar to the Harvard RoboFly that accomplished the first takeoff of an insect scale flapping wing aircraft, except that it is equipped with independently actuated wings and the vehicle center-of-gravity can be manipulated for control purposes. Using the results from the derivation of the aerodynamic forces and moments from Part I, a control allocation strategy and a feedback control law are designed that enables the vehicle to achieve untethered, stabilized flight about a hover condition. The control laws are designed to make use of three actuators, two of which control the angular position of the wing in the stroke plane, and one that moves a bob-weight that manipulates the vehicle center-of-gravity. The Split-Cycle Constant-Period Frequency Modulation technique, introduced in Part I, is used to allow each wing to generate non-zero cycle-averaged rolling and yawing moments. The technique achieves this objective by varying the frequency of the oscillators, that drive each wing throughout the wing-beat cycles, such that the dynamic pressure acting on each wing during the upstroke is different from that which acts on the

[*]Senior Electronics Engineer, Control Design and Analysis Branch, 2210 Eighth Street, Ste 21, Air Force Research Laboratory, WPAFB, OH 45433-7531 Email Michael.Oppenheimer@wpafb.af.mil, Ph. (937) 255-8490, Fax (937) 656-4000, Senior Member, AIAA

[†]Senior Aerospace Engineer, Control Design and Analysis Branch, 2210 Eighth Street, Ste. 21, Air Force Research Laboratory, WPAFB, OH 45433-7531 Email David.Doman@wpafb.af.mil, Ph. (937) 255-8451, Fax (937) 656-4000, Associate Fellow AIAA

[‡]Electronics Engineer, Control Design and Analysis Branch, 2210 Eighth Street, Ste 21, Air Force Research Laboratory, WPAFB, OH 45433-7531 Email David.Sigthorsson@afmcx.net, Ph. (937) 255-9707, Fax (937) 656-4000. This research was performed while this author held a National Research Council Research Associateship Award at the Air Force Research Laboratory.

wing during the downstroke. Pitching moment and high speed translation are controlled by varying the vehicle center-of-gravity using a bob-weight actuator.

I.   Introduction

In Part I[1] of this series, expressions for the instantaneous and cycle averaged aerodynamic forces and moments of a flapping wing biomimetic vehicle, with features similar to the Harvard Robofly described by Wood,[2] were derived. The proposed vehicle makes use of three actuators, two of which are used to independently vary the position of the wing spars in the stroke plane, while the third is used to control the position of a bob-weight. The planforms are free to passively rotate about the spar within limits prescribed by a specially designed hinge, the details of which, are provided in Part I of this series. Because of the limited number of actuators and the periodic nature of the aerodynamic forces and moments, a control strategy has been devised that will allow 5 degree of freedom control of the fuselage to be achieved. The split-cycle constant-period frequency modulation method that enables this motion is a method which allows the frequency of the oscillator that controls the instantaneous wing position to be varied at the endpoints of each stroke, in such a way as to preserve the period of a temporally symmetric wing beat. Thus, the angular velocity and dynamic pressure can be varied throughout each cycle. This feature enables asymmetric cycle averaged forces and moments to be generated that can be used for maneuvering and control. There are two input parameters to each wing beat waveform generator. These parameters are called the fundamental wing beat frequencies, ω_{LW} and ω_{RW}, and the split-cycle parameters, δ_{LW} and δ_{RW}. The fundamental frequency controls the frequency of the temporally symmetric portions of the wing beat, while the split-cycle parameters control the temporally asymmetric portions of the wing beat.

In the present paper, the analysis that was started in Part I is continued by describing the split-cycle formulation and analyzing the effects of a bob-weight upon the body-axis forces and moments. Expressions for the control derivatives of the cycle-averaged forces and moments associated with variations in the fundamental wing beat frequencies, split-cycle parameters, and bob-weight position are derived. The expressions are linearized about a hover flight condition and a control allocation strategy is proposed. A flight control law is formulated based on the linearized cycle-averaged model, and is implemented on a dynamic model that includes instantaneous variations in the forces and moments to verify the efficacy of the cycle-average based control design. Areas where dynamics and control can influence the design of the aircraft are highlighted throughout the paper.

II. Equations of Motion

A standard set of 6 degree-of-freedom rigid body equations of motion are employed.[3] These are the same equations that describe the motion of a rigid body aircraft; however, because the angle of each wing in the stroke plane is a periodic function of time, the forces and moments that drive the equations consist of multiple, independent, and variable periodic functions of time. We assume that the wings are massless; therefore, there exists no inertial coupling between the fuselage and the wings. We expect that the inertial coupling between the wings and body will be small because in the Harvard Robofly, the wings constitute less than 1% of the total vehicle weight.[2] The equations of motion are

$$
\begin{bmatrix} \dot{p} \\ \dot{q} \\ \dot{r} \end{bmatrix} = \mathbf{I}^{-1} \left(\begin{bmatrix} L \\ M \\ N \end{bmatrix} - \boldsymbol{\omega} \times \mathbf{I}\boldsymbol{\omega} \right) \tag{1}
$$

$$
\begin{bmatrix} \dot{u} \\ \dot{v} \\ \dot{w} \end{bmatrix} = \begin{bmatrix} qw - rv \\ ru - pw \\ pv - qu \end{bmatrix} + \begin{bmatrix} X/m \\ Y/m \\ Z/m \end{bmatrix} - \mathbf{R}_I^B \begin{bmatrix} -g \\ 0 \\ 0 \end{bmatrix} \tag{2}
$$

$$
\begin{bmatrix} \dot{x} \\ \dot{y} \\ \dot{z} \end{bmatrix} = \mathbf{R}_B^I \begin{bmatrix} u \\ v \\ w \end{bmatrix} \tag{3}
$$

$$
\begin{bmatrix} \dot{q}_0 \\ \dot{q}_1 \\ \dot{q}_2 \\ \dot{q}_3 \end{bmatrix} = \begin{bmatrix} 0 & -p & -q & -r \\ p & 0 & r & -q \\ q & -r & 0 & p \\ r & q & -p & 0 \end{bmatrix} \begin{bmatrix} q_0 \\ q_1 \\ q_2 \\ q_3 \end{bmatrix} \tag{4}
$$

where $\mathbf{I}$ is the inertia matrix, $\boldsymbol{\omega} = [p\,q\,r]$ is the angular rate vector, L, M, N are the rolling, pitching, and yawing moments, u, v, w are the translation velocities, X, Y, Z are the body axes forces, m is the vehicle mass, g is the acceleration of gravity, x, y, z are the vehicle positions with respect to an inertial frame, and $\mathbf{q} = q_0 + q_1\hat{i} + q_2\hat{j} + q_3\hat{k}$ is a quaternion used to perform the 3-2-1 standard Euler transformation. Also, $\mathbf{R}_B^I = \mathbf{R}_I^{B^T}$ are rotation matrices that transform from body to inertial axes and back. The equations of motion are driven by the instantaneous forces and moments presented in Part I[1] of this series. These blade element based aerodynamic forces and moments do not account for leading-edge vortex effects and the effects of wake-capture that have been observed in experiments and therefore, in practice, there exists a significant amount of uncertainty that must be accommodated by

any feedback controller designed based on blade-element results.

III.   Split-Cycle Fundamentals

Varying the fundamental wing beat frequency allows control over the translational and rotational degrees of freedom of the vehicle. When the split-cycle parameters δ_{LW} and δ_{RW} are zero, the left and right wings beat symmetrically and multi-axis control of the vehicle is not possible. This section describes the split-cycle parameters and shows how the wing beat frequency is modified for the upstroke and downstroke.

The fundamental idea is to piece together two cosine waves of different frequencies over one complete wing beat cycle. Either the upstroke or the downstroke will be impeded, while the opposite stoke is advanced. The development of the split-cycle parameters for the right wing is exactly the same as for the left wing. Therefore, the subscripts for right wing and left wing will be eliminated in the following derivations.

For the first half of the cycle, the frequency is altered from ω to $\omega - \delta$. Thus, the position of the wing during the upstroke is defined by

$$\phi_U = \cos\left[(\omega - \delta)\, t\right] \tag{5}$$

where δ is the split-cycle parameter and ω is the symmetric or fundamental wing beat frequency. For $\delta > 0$, this would produce an impeded or lower frequency upstroke, as compared to the fundamental wing beat frequency. For the downstroke, the position of the wing becomes

$$\phi_D = \cos\left[(\omega + \sigma)\, t\right] \tag{6}$$

where σ is the frequency modification parameter, which is dependent upon δ. In order to compute the fundamental frequency change for the second half of the cycle, recall that the combination of the two altered frequency strokes must have the same period as the unaltered frequency stroke. Then, for an upstroke frequency of $\omega - \delta$ and a downstroke frequency of $\omega + \sigma$, the requirement becomes

$$T_U + T_D = T \tag{7}$$

where $T_U = \frac{2\pi}{\omega - \delta}$ is the period of the upstroke, $T_D = \frac{2\pi}{\omega + \sigma}$ is the period of the downstroke, and $T = \frac{2\pi}{\omega}$ is the full cycle period. Since the upstroke and downstroke only occur for one-half of their respective periods, Equation 7 becomes

$$\frac{1}{2}\left(\frac{2\pi}{\omega - \delta}\right) + \frac{1}{2}\left(\frac{2\pi}{\omega + \sigma}\right) = \frac{2\pi}{\omega} \tag{8}$$

Solving for σ yields

$$\sigma = \frac{\delta\omega}{\omega - 2\delta} \tag{9}$$

Equation 9 shows that σ is a function of the symmetric frequency, ω, and the split-cycle parameter, δ. Thus, split-cycle frequency modulation is fully defined by the parameter δ.

There are two equations that provide limits on δ, namely,

$$\omega - \delta > 0 \quad \omega + \sigma > 0 \tag{10}$$

Equation 10 ensures that the wing beat frequencies are always positive. The first part reduces to $\delta < \omega$. For the second part, substitute Equation 9 into Equation 10 and simplify to obtain the following condition

$$\frac{\omega(\omega - \delta)}{\omega - 2\delta} > 0 \tag{11}$$

Three cases occur here. Note that the numerator of Equation 11 is always positive since $\delta < \omega$ and $\omega > 0$. Consider the denominator of Equation 11. Case 1 is for $\delta > \frac{\omega}{2}$.

$$\delta > \frac{\omega}{2} \;\rightarrow\; \omega - 2\delta < 0 \;\rightarrow\; \omega + \sigma < 0 \tag{12}$$

Obviously, the frequency of the downstroke cannot be less than zero and, therefore, δ cannot be larger than $\frac{\omega}{2}$. Case 2 is for $\delta = \frac{\omega}{2}$. Then,

$$\delta = \frac{\omega}{2} \;\rightarrow\; \omega - 2\delta = 0 \;\rightarrow\; \omega + \sigma = \infty \tag{13}$$

As with case 1, case 2 yields an unrealistic result. Case 3 is for $\delta < \frac{\omega}{2}$. Then,

$$\delta < \frac{\omega}{2} \;\rightarrow\; \omega - 2\delta > 0 \;\rightarrow\; \omega + \sigma > 0 \tag{14}$$

For case 3, the frequency of the downstroke is larger than zero, as required. Since this requirement, namely, $\delta < \frac{\omega}{2}$, is more restrictive than that obtained from the first part of Equation 10, we conclude that δ must satisy

$$\delta < \frac{\omega}{2} \tag{15}$$

If $\delta = 0$, the fundamental wing beat frequency for both the upstroke and downstroke is achieved.

It should be noted that $\delta < 0$ is also an option. In this case, the upstroke is advanced and the downstroke is impeded (just the opposite of the $\delta > 0$ case). There is no lower limit on δ, which can again be determined using Equation 10. Clearly, for $\delta < 0$, the first part of

Equation 10 is satisfied. Consider the following for the $\omega + \sigma > 0$ requirement:

$$\lim_{\delta \to -\infty} \sigma = \lim_{\delta \to -\infty} \frac{\delta\omega}{\omega - 2\delta} = \lim_{\delta \to -\infty} \frac{\delta\omega}{-2\delta} = \frac{-\omega}{2} \tag{16}$$

Then,

$$\lim_{\delta \to -\infty} \omega + \sigma = \omega - \frac{\omega}{2} = \frac{\omega}{2} \tag{17}$$

and thus, the downstroke frequency is greater than zero for any $\delta < 0$. Therefore, the only active constraint for the split-cycle is $\delta < \frac{\omega}{2}$.

One other requirement needs to be taken into account. Equation 6 must to be modified to ensure that the split-cycle wing position is continuous. In other words, the wing position at the end of the upstroke must equal the wing position at the beginning of the downstroke. The upstroke ends at time $t = \frac{\pi}{\omega - \delta}$. Substituting this time into Equation 5 yields

$$\phi_U|_{t=\frac{\pi}{\omega-\delta}} = \cos\left[(\omega - \delta)\frac{\pi}{\omega - \delta}\right] = \cos\pi = -1 \tag{18}$$

Evaluating Equation 6 at this time produces

$$\phi_D|_{t=\frac{\pi}{\omega-\delta}} = \cos\left[(\omega + \sigma)\frac{\pi}{\omega - \delta}\right] = \cos\left[\frac{\omega(\omega - \delta)}{\omega - 2\delta}\left(\frac{\pi}{\omega - \delta}\right)\right] = \cos\left[\frac{\omega\pi}{\omega - 2\delta}\right] \tag{19}$$

Considering the argument of the cosine function and setting it equal to π (the result of Equation 18) gives

$$\frac{\omega\pi}{\omega - 2\delta} = \pi \quad \to \quad 2\delta\pi = 0 \quad \to \quad \delta = 0 \tag{20}$$

Hence, there will be a mismatch of wing positions at the transition from the upstroke to the downstroke if $\delta \neq 0$. To eliminate this, the downstroke can be phase shifted. The form of the downstroke wing position function is altered from Equation 6 to

$$\phi_D = \cos\left[(\omega + \sigma)t + \xi\right] \tag{21}$$

Evaluating Equation 21 at time $t = \frac{\pi}{\omega - \delta}$ produces

$$\phi_D|_{t=\frac{\pi}{\omega-\delta}} = \cos\left[(\omega + \sigma)\frac{\pi}{\omega - \delta} + \xi\right] = \cos\left[\frac{\omega(\omega - \delta)}{\omega - 2\delta}\left(\frac{\pi}{\omega - \delta}\right) + \xi\right] = \cos\left[\frac{\omega\pi}{\omega - 2\delta} + \xi\right] \tag{22}$$

Setting the argument of the cosine in Equation 22 equal to π produces

$$\frac{\omega\pi}{\omega - 2\delta} + \xi = \pi \quad \to \quad \xi = \frac{-2\pi\delta}{\omega - 2\delta} \tag{23}$$

Utilizing the phase shift in Equation 23 guarantees that the wing position at the end of the

upstroke is equal to the wing position at the beginning of the downstroke.

In summary, the upstroke and downstroke wing positions are given by

$$\phi_U = \cos\left[(\omega - \delta)\,t\right] \tag{24}$$

$$\phi_D = \cos\left[(\omega + \sigma)\,t + \xi\right] \tag{25}$$

where $\sigma = \frac{\delta\omega}{\omega - 2\delta}$ and $\xi = \frac{-2\pi\delta}{\omega - 2\delta}$. The requirement on the split-cycle parameter is

$$\delta < \frac{w}{2} \tag{26}$$

and δ can take on any negative value.

Figures 1 and 2 show wing beat patterns for $\delta > 0$ and $\delta < 0$ along with a symmetric wing beat. In Figure 1, the upstroke is impeded, while the downstroke is advanced, while in Figure 2, the upstroke is advanced and the downstroke is impeded. The split-cycle parameter, δ, along with ω for the right wing and left wing become control parameters in the control law. Hence, the wing position control parameters are ω_{RW}, ω_{LW}, δ_{RW}, and δ_{LW}. For utilization in a control law, the control derivatives associated with the fundamental and split-cycle frequencies must be evaluated. The next section addresses this task.
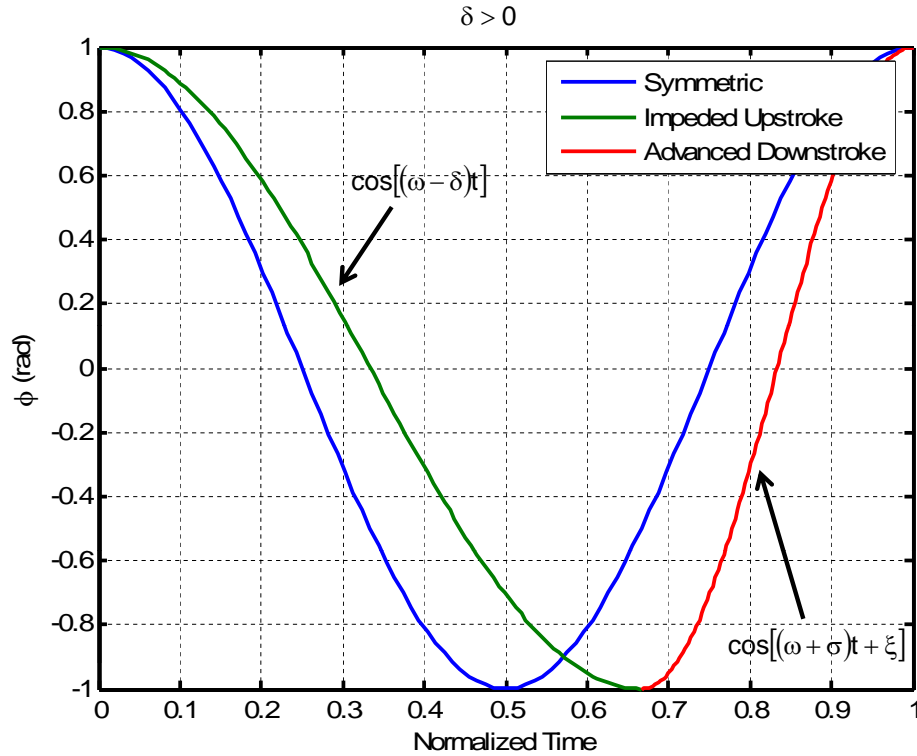

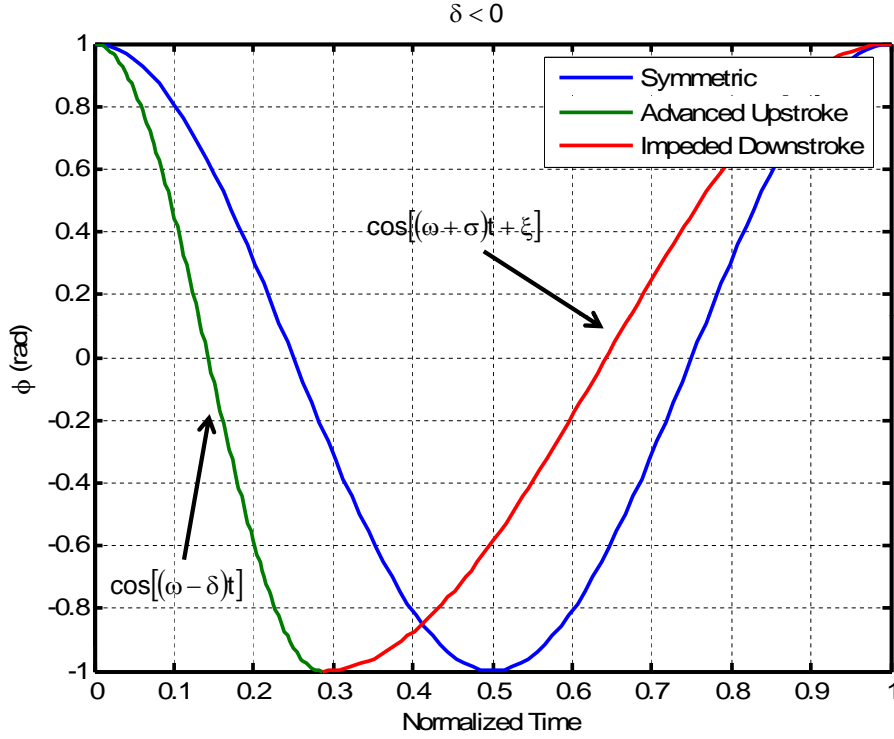**Figure 1. Split-cycle results for $\delta > 0$.**

Figure 2. Split-cycle results for $\delta < 0$.

IV.   Control Derivatives

The parameters used to control the aerodynamic forces and moments are the fundamental wing beat frequencies, ω_{RW} and ω_{LW}, and the split-cycle parameters, δ_{RW} and δ_{LW}. For controllability analysis and control synthesis, the sensitivity of each cycle-averaged generalized force to each control input parameter must be determined.

A.   General Aerodynamic Control Derivative Expressions

The partial derivatives of each cycle-averaged force and moment, derived in Part-I, with respect to each wing beat control input parameter are provided below

$$\frac{\partial \overline{F}_{x\,RW}^{B}}{\partial \delta_{RW}} = \frac{k_L \omega_{RW} \delta_{RW} (\omega_{RW} - \delta_{RW})}{(\omega_{RW} - 2\delta_{RW})^2} \tag{27}$$

$$\frac{\partial \overline{F}_{x\,RW}^{B}}{\partial \omega_{RW}} = \frac{k_L (\omega_{RW}^3 - 4\delta_{RW}\omega_{RW}^2 + 4\omega_{RW}\delta_{RW}^2 - \delta_{RW}^3)}{(\omega_{RW} - 2\delta_{RW})^2} \tag{28}$$

$$\frac{\partial \overline{F_{xLW}}^B}{\partial \delta_{LW}} = \frac{k_L \omega_{LW} \delta_{LW}(\omega_{LW} - \delta_{LW})}{(\omega_{LW} - 2\delta_{LW})^2} \tag{29}$$

$$\frac{\partial \overline{F_{xLW}}^B}{\partial \omega_{LW}} = \frac{k_L(\omega_{LW}^3 - 4\delta_{LW}\omega_{LW}^2 + 4\omega_{LW}\delta_{LW}^2 - \delta_{LW}^3)}{(\omega_{LW} - 2\delta_{LW})^2} \tag{30}$$

$$\frac{\partial \overline{F_{yRW}}^B}{\partial \omega_{RW}} = \frac{\partial \overline{F_{yRW}}^B}{\partial \delta_{RW}} = \frac{\partial \overline{F_{yLW}}^B}{\partial \omega_{LW}} = \frac{\partial \overline{F_{yLW}}^B}{\partial \delta_{LW}} = 0 \tag{31}$$

$$\frac{\partial \overline{F_{zRW}}^B}{\partial \delta_{RW}} = \frac{-k_D J_1(1)\omega_{RW}(\omega_{RW}^2 - 2\delta_{RW}\omega_{RW} + 2\delta_{RW}^2)}{(\omega_{RW} - 2\delta_{RW})^2} \tag{32}$$

$$\frac{\partial \overline{F_{zRW}}^B}{\partial \omega_{RW}} = \frac{-k_D J_1(1)\delta_{RW}(\omega_{RW}^2 - 4\delta_{RW}\omega_{RW} + 2\delta_{RW}^2)}{(\omega_{RW} - 2\delta_{RW})^2} \tag{33}$$

$$\frac{\partial \overline{F_{zLW}}^B}{\partial \delta_{LW}} = \frac{-k_D J_1(1)\omega_{LW}(\omega_{LW}^2 - 2\delta_{LW}\omega_{LW} + 2\delta_{LW}^2)}{(\omega_{LW} - 2\delta_{LW})^2} \tag{34}$$

$$\frac{\partial \overline{F_{zLW}}^B}{\partial \omega_{LW}} = \frac{-k_D J_1(1)\delta_{LW}(\omega_{LW}^2 - 4\delta_{LW}\omega_{LW} + 2\delta_{LW}^2)}{(\omega_{LW} - 2\delta_{LW})^2} \tag{35}$$

$$\frac{\partial \overline{M_{xRW}}^B}{\partial \delta_{RW}} = \frac{-k_D \omega_{RW}(y_{cp}^{WP} + w J_1(1))(\omega_{RW}^2 - 2\delta_{RW}\omega_{RW} + 2\delta_{RW}^2)}{2(\omega_{RW} - 2\delta_{RW})^2} \tag{36}$$

$$\frac{\partial \overline{M_{xRW}}^B}{\partial \omega_{RW}} = \frac{-k_D \delta_{RW}(y_{cp}^{WP} + w J_1(1))(\omega_{RW}^2 - 4\delta_{RW}\omega_{RW} + 2\delta_{RW}^2)}{2(\omega_{RW} - 2\delta_{RW})^2} \tag{37}$$

$$\frac{\partial \overline{M_{xLW}}^B}{\partial \delta_{LW}} = \frac{k_D \omega_{LW}(y_{cp}^{WP} + w J_1(1))(\omega_{LW}^2 - 2\delta_{LW}\omega_{LW} + 2\delta_{LW}^2)}{2(\omega_{LW} - 2\delta_{LW})^2} \tag{38}$$

$$\frac{\partial \overline{M_{xLW}}^B}{\partial \omega_{LW}} = \frac{k_D \delta_{LW}(y_{cp}^{WP} + w J_1(1))(\omega_{LW}^2 - 4\delta_{LW}\omega_{LW} + 2\delta_{LW}^2)}{2(\omega_{LW} - 2\delta_{LW})^2} \tag{39}$$

$$\frac{\partial \overline{M_{yRW}}^B}{\partial \delta_{RW}} = \frac{J_1(1)\omega_{RW}\left[k_L x_{cp}^{WP}\cos\alpha + k_D x_{cp}^{WP}\sin\alpha + k_D \Delta x_R^B\right](2\delta_{RW}^2 - 2\delta_{RW}\omega_{RW} + \omega_{RW}^2)}{(\omega_{RW} - 2\delta_{RW})^2} - \frac{k_L \Delta z_R^B \delta_{RW}\omega_{RW}(\omega_{RW} - \delta_{RW})}{(\omega_{RW} - 2\delta_{RW})^2} \tag{40}$$

$$\frac{\partial \overline{M_{yRW}}^B}{\partial \omega_{RW}} = \frac{J_1(1)\delta_{RW}\left[k_L x_{cp}^{WP}\cos\alpha + k_D x_{cp}^{WP}\sin\alpha + k_D \Delta x_R^B\right](2\delta_{RW}^2 - 4\delta_{RW}\omega_{RW} + \omega_{RW}^2)}{(\omega_{RW} - 2\delta_{RW})^2} - \frac{k_L \Delta z_R^B(\delta_{RW}^3 - 4\delta_{RW}^2\omega_{RW} + 4\delta_{RW}\omega_{RW}^2 - \omega_{RW}^3)}{(\omega_{RW} - 2\delta_{RW})^2} \tag{41}$$

$$\frac{\partial \overline{M}_{y\,LW}^{B}}{\partial \delta_{LW}} = \frac{J_1(1)\omega_{LW}\left[k_L x_{cp}^{WP}\cos\alpha + k_D x_{cp}^{WP}\sin\alpha + k_D\Delta x_L^B\right](2\delta_{LW}^2 - 2\delta_{LW}\omega_{LW} + \omega_{LW}^2)}{(\omega_{LW} - 2\delta_{LW})^2} - \frac{k_L\Delta z_L^B\delta_{LW}\omega_{LW}(\omega_{LW} - \delta_{LW})}{(\omega_{LW} - 2\delta_{LW})^2}$$

$$(42)$$

$$\frac{\partial \overline{M}_{y\,LW}^{B}}{\partial \omega_{LW}} = \frac{J_1(1)\delta_{LW}\left[k_L x_{cp}^{WP}\cos\alpha + k_D x_{cp}^{WP}\sin\alpha + k_D\Delta x_L^B\right](2\delta_{LW}^2 - 4\delta_{LW}\omega_{LW} + \omega_{LW}^2)}{(\omega_{LW} - 2\delta_{LW})^2} - \frac{k_L\Delta z_L^B(\delta_{LW}^3 - 4\delta_{LW}^2\omega_{LW} + 4\delta_{LW}\omega_{LW}^2 - \omega_{LW}^3)}{(\omega_{LW} - 2\delta_{LW})^2}$$

$$(43)$$

$$\frac{\partial \overline{M}_{z\,RW}^{B}}{\partial \delta_{RW}} = \frac{-2k_L(y_{cp}^{WP}J_1(1) + \frac{w}{4})\omega_{RW}\delta_{RW}(\omega_{RW} - \delta_{RW})}{(\omega_{RW} - 2\delta_{RW})^2} \qquad (44)$$

$$\frac{\partial \overline{M}_{z\,RW}^{B}}{\partial \omega_{RW}} = \frac{-2k_L(y_{cp}^{WP}J_1(1) + \frac{w}{4})(\omega_{RW}^3 - 4\delta_{RW}\omega_{RW}^2 + 4\omega_{RW}\delta_{RW}^2 - \delta_{RW}^3)}{(\omega_{RW} - 2\delta_{RW})^2} \qquad (45)$$

$$\frac{\partial \overline{M}_{z\,LW}^{B}}{\partial \delta_{LW}} = \frac{2k_L(y_{cp}^{WP}J_1(1) + \frac{w}{4})\omega_{LW}\delta_{LW}(\omega_{LW} - \delta_{LW})}{(\omega_{LW} - 2\delta_{LW})^2} \qquad (46)$$

$$\frac{\partial \overline{M}_{z\,RW}^{B}}{\partial \omega_{LW}} = \frac{2k_L(y_{cp}^{WP}J_1(1) + \frac{w}{4})(\omega_{LW}^3 - 4\delta_{LW}\omega_{LW}^2 + 4\omega_{LW}\delta_{LW}^2 - \delta_{LW}^3)}{(\omega_{LW} - 2\delta_{LW})^2} \qquad (47)$$

B. Aerodynamic Control Derivatives about Hover

The control of this vehicle in the vicinity of hover is of considerable interest. Therefore, the control derivatives at the hover condition where $\omega_{RW} = \omega_{LW} = \omega_o$ and $\delta_{RW} = \delta_{LW} = 0$ are evaluated, where $\omega_o = \sqrt{\frac{mg}{0.5\rho C_L(\alpha)I_A}}$. Of course, this condition assumes that the nominal center-of-gravity of the vehicle and wing root hinges are aligned such that $\Delta z_R^B = \Delta z_L^B = 0$. The control derivatives about hover are presented in Table 1.

Control Derivative $\frac{\partial \overline{G}}{\partial \bullet}\big|_{\omega=\omega_o, \delta=0}$
$\frac{\partial \overline{F_x}_{RW}^B}{\partial \delta_{RW}}\bigg|_{\omega_{RW}=\omega_o, \delta_{RW}=0} = 0$
$\frac{\partial \overline{F_x}_{RW}^B}{\partial \omega_{RW}}\bigg|_{\omega_{RW}=\omega_o, \delta_{RW}=0} = k_L \omega_o$
$\frac{\partial \overline{F_x}_{LW}^B}{\partial \delta_{LW}}\bigg|_{\omega_{LW}=\omega_o, \delta_{LW}=0} = 0$
$\frac{\partial \overline{F_x}_{LW}^B}{\partial \omega_{LW}}\bigg|_{\omega_{LW}=\omega_o, \delta_{LW}=0} = k_L \omega_o$
$\frac{\partial \overline{F_y}_{RW}^B}{\partial \omega_{RW}} = \frac{\partial \overline{F_y}_{RW}^B}{\partial \delta_{RW}} = \frac{\partial \overline{F_y}_{LW}^B}{\partial \omega_{LW}} = \frac{\partial \overline{F_y}_{LW}^B}{\partial \delta_{LW}} = 0$
$\frac{\partial \overline{F_z}_{RW}^B}{\partial \delta_{RW}}\bigg|_{\omega_{RW}=\omega_o, \delta_{RW}=0} = -k_D J_1(1)\omega_o$
$\frac{\partial \overline{F_z}_{RW}^B}{\partial \omega_{RW}}\bigg|_{\omega_{RW}=\omega_o, \delta_{RW}=0} = 0$
$\frac{\partial \overline{F_z}_{LW}^B}{\partial \delta_{LW}}\bigg|_{\omega_{LW}=\omega_o, \delta_{LW}=0} = -k_D J_1(1)\omega_o$
$\frac{\partial \overline{F_z}_{LW}^B}{\partial \omega_{LW}}\bigg|_{\omega_{LW}=\omega_o, \delta_{LW}=0} = 0$
$\frac{\partial \overline{M_x}_{RW}^B}{\partial \delta_{RW}}\bigg|_{\omega_{RW}=\omega_o, \delta_{RW}=0} = -\frac{1}{2}k_D \omega_o(y_{cp}^{WP} + w J_1(1))$
$\frac{\partial \overline{M_x}_{RW}^B}{\partial \omega_{RW}}\bigg|_{\omega_{RW}=\omega_o, \delta_{RW}=0} = 0$
$\frac{\partial \overline{M_x}_{LW}^B}{\partial \delta_{LW}}\bigg|_{\omega_{LW}=\omega_o, \delta_{LW}=0} = \frac{1}{2}k_D \omega_o(y_{cp}^{WP} + w J_1(1))$
$\frac{\partial \overline{M_x}_{LW}^B}{\partial \omega_{LW}}\bigg|_{\omega_{LW}=\omega_o, \delta_{LW}=0} = 0$
$\frac{\partial \overline{M_y}_{RW}^B}{\partial \delta_{RW}}\bigg|_{\omega_{RW}=\omega_o, \delta_{RW}=0} = J_1(1)\omega_o \left[k_L x_{cp}^{WP} \cos\alpha + k_D(x_{cp}^{WP} \sin\alpha + \Delta x_R^B) \right]$
$\frac{\partial \overline{M_y}_{RW}^B}{\partial \omega_{RW}}\bigg|_{\omega_{RW}=\omega_o, \delta_{RW}=0} = k_L \Delta z_R^B \omega_o = 0 \text{ for } \Delta z_R^B = 0$
$\frac{\partial \overline{M_y}_{LW}^B}{\partial \delta_{LW}}\bigg|_{\omega_{LW}=\omega_o, \delta_{LW}=0} = J_1(1)\omega_o \left[k_L x_{cp}^{WP} \cos\alpha + k_D(x_{cp}^{WP} \sin\alpha + \Delta x_L^B) \right]$
$\frac{\partial \overline{M_y}_{LW}^B}{\partial \omega_{LW}}\bigg|_{\omega_{LW}=\omega_o, \delta_{LW}=0} = k_L \Delta z_L^B \omega_o = 0 \text{ for } \Delta z_L^B = 0$
$\frac{\partial \overline{M_z}_{RW}^B}{\partial \delta_{RW}}\bigg|_{\omega_{RW}=\omega_o, \delta_{RW}=0} = 0$
$\frac{\partial \overline{M_z}_{RW}^B}{\partial \omega_{RW}}\bigg|_{\omega_{RW}=\omega_o, \delta_{RW}=0} = -2k_L \omega_o \left[y_{cp}^{WP} J_1(1) + \frac{w}{4} \right]$
$\frac{\partial \overline{M_z}_{LW}^B}{\partial \delta_{LW}}\bigg|_{\omega_{LW}=\omega_o, \delta_{LW}=0} = 0$
$\frac{\partial \overline{M_z}_{LW}^B}{\partial \omega_{LW}}\bigg|_{\omega_{LW}=\omega_o, \delta_{LW}=0} = 2k_L \omega_o \left[y_{cp}^{WP} J_1(1) + \frac{w}{4} \right]$

Table 1. Aerodynamic control derivatives about hover.

C. Bob-weight Control Derivatives

It is important to note that variations in symmetric and split cycle frequency parameters are not effective in generating independent changes to the pitching moment. Using only the aerodynamic control input parameters, changes in pitching moment are accompanied by undesirable changes in other forces and moments. It is for this reason that the bob-weight actuator is introduced. The bob-weight is taken to lie in the vehicle plane of symmetry and at zero deflection is coincident with the center-of-gravity of the vehicle without the bob-weight. The bob-weight need not be dead-weight. Any necessary vehicle component that is not sensitive to movement could serve the purpose, e.g., battery, power converter, etc. The weight would be mounted near the tip of a bimorph piezoelectric actuator. The tip deflection is designed to primarily consist of translation in the z-body axis direction, while translation in the x-body direction would be so small as to be negligible. Hence, the bob-weight motion is constrained to be an arc in the x_b, z_b plane.

Let m_o be the total vehicle mass exclusive of the bob-weight and bob-weight actuator and $x_{cg_o}^B, 0, z_{cg_o}^B$ be the location of the center of mass in body coordinates. Let m_{BW} denote the mass of the bob-weight and actuator assembly and $x_{BW}^B, 0, z_{BW}^B$ be the location of the center of mass of this assembly in body coordinates. Because motion is constrained to an arc in the x_b, z_b plane, the y-body locations of these centers-of-mass are zero, that is, no out of plane motion occurs and the radius of the arc at the tip of the actuator is large relative to the tip displacement. Because of the nature of the tip motion of the bimorph actuator, it is assumed that motion of the bob-weight does not alter the x-location of the center of mass of the bob-weight assembly, hence, x_{BW}^B is constant. Defining $x_{cg}^B, 0, z_{cg}^B$ as the location of the center of mass of the entire vehicle, including the bob-weight, this assumption implies that x_{cg}^B is fixed for a given bob-weight mass. Wood[2] indicates that the mass of each wing is less than 1% of the gross vehicle weight; therefore, it is also assumed that the mass of each wing is negligible. Under the above conditions, the x- and z-body locations of the center of mass are given by

$$x_{cg}^B = \frac{x_{cg_o}^B m_o + x_{BW}^B m_{BW}}{m_o + m_{BW}} \tag{48}$$

$$z_{cg}^B = \frac{z_{cg_o}^B m_o + z_{BW}^B m_{BW}}{m_o + m_{BW}} \tag{49}$$

Again, for a fixed bob-weight mass, the x location of the center of mass is independent of the movement of the bob-weight. It is important to note that the aerodynamic moments are taken about the body-frame and are independent of the center-of-gravity location, even when the center-of-gravity is not coincident with the origin of the body-axes system. Therefore, the moments about the body-axes are comprised of aerodynamic moments and moments due to center-of-gravity offset. In other words, the total cycle-averaged moment about the

body-axes coordinate system, $\overline{\mathbf{M}}^{\mathbf{B}}$, become

$$\overline{\mathbf{M}}^{\mathbf{B}} = \overline{\mathbf{M}}^{\mathbf{B}}_{\mathbf{aero}} + \overline{\mathbf{M}}^{\mathbf{B}}_{\mathbf{cg}} \tag{50}$$

where $\overline{\mathbf{M}}^{\mathbf{B}}_{\mathbf{aero}}$ is the cycle-averaged moment produced by the wings and $\overline{\mathbf{M}}^{\mathbf{B}}_{\mathbf{cg}}$ is the cycle-averaged moment due to center-of-gravity offset from the origin of the body-axes. The cycle-averaged moment due to center-of-gravity offset is

$$\overline{\mathbf{M}}^{\mathbf{B}}_{\mathbf{cg}} = \frac{\omega}{2\pi} \int_0^{\frac{2\pi}{\omega}} \mathbf{r}^{\mathbf{B}}_{\mathbf{cg}} \times \mathbf{F}^{\mathbf{B}}_{\mathbf{cg}} \, dt \tag{51}$$

where the integral of each component of the integrand is evaluated and $\mathbf{r}^{\mathbf{B}}_{\mathbf{cg}} = \begin{bmatrix} x^B_{cg} & 0 & z^B_{cg} \end{bmatrix}$ is the position vector from the center-of-gravity to the origin of the body-axes system and x^B_{cg}, z^B_{cg} are provided in Equations 48 and 49. The force is gravitational and can be written as

$$\mathbf{F}^{\mathbf{B}}_{\mathbf{cg}} = \mathbf{R}^{\mathbf{B}}_{\mathbf{I}} \begin{bmatrix} -(m_o + m_{BW})\, g & 0 & 0 \end{bmatrix} \tag{52}$$

where $\mathbf{R}^{\mathbf{B}}_{\mathbf{I}}$ is a rotation matrix from the inertial frame to the body frame and g is the acceleration due to gravity. Let this force, in general, be represented as $\mathbf{F}^{\mathbf{B}}_{\mathbf{cg}} = \begin{bmatrix} F^B_{x_{cg}} & F^B_{y_{cg}} & F^B_{z_{cg}} \end{bmatrix}$. Then, by performing the cross product operation, the moment due to center-of-gravity offset is

$$\overline{\mathbf{M}}^{\mathbf{B}}_{\mathbf{cg}} = \frac{\omega}{2\pi} \int_0^{\frac{2\pi}{\omega}} \begin{bmatrix} -z^B_{cg} F^B_{y_{cg}} \\ z^B_{cg} F^B_{x_{cg}} - x^B_{cg} F^B_{z_{cg}} \\ x^B_{cg} F^B_{y_{cg}} \end{bmatrix} dt \tag{53}$$

Assume that the position vector and force in Equation 52 are constant over a full wing beat cycle. In light of these assumptions, the cycle-averaged moments, computed by evaluating the integrals in Equation 53 are

$$\overline{\mathbf{M}}^{\mathbf{B}}_{\mathbf{cg}} = \begin{bmatrix} -z^B_{cg} F^B_{y_{cg}} \\ z^B_{cg} F^B_{x_{cg}} - x^B_{cg} F^B_{z_{cg}} \\ x^B_{cg} F^B_{y_{cg}} \end{bmatrix} \tag{54}$$

It is assumed that a linear relationship exists between the voltage applied to the bob-weight actuator, V_{BW}, and the bob-weight tip deflection. Therefore,

$$\frac{\partial z^B_{BW}}{\partial V_{BW}} = k_{BW} \tag{55}$$

Additionally, since it is assumed that x^B_{BW} is a constant, $\frac{\partial z^B_{BW}}{\partial V_{BW}} = 0$. Then, the control

effectiveness of the bob-weight actuator can be expressed as

$$\frac{\partial \overline{\mathbf{M}}_{\mathbf{cg}}^{\mathbf{B}}}{\partial V_{BW}} = \frac{\partial \overline{\mathbf{M}}_{\mathbf{cg}}^{\mathbf{B}}}{\partial z_{BW}^{B}} \frac{\partial z_{BW}}{\partial V_{BW}} \tag{56}$$

Substituting Equation 49 into Equation 53 and computing the derivatives as specified in Equation 56 yields

$$\frac{\partial \overline{\mathbf{M}}_{\mathbf{cg}}^{\mathbf{B}}}{\partial V_{BW}} = \begin{pmatrix} \frac{-m_{BW}}{m_o + m_{BW}} F_{y_{cg}}^{B} k_{BW} \\ \frac{m_{BW}}{m_o + m_{BW}} F_{x_{cg}}^{B} k_{BW} \\ 0 \end{pmatrix} \tag{57}$$

Note that when the body axis system is aligned with the inertial axis system, the attitudes of the vehicle are zero and $\mathbf{R_I^B} = \mathbf{I}$. Thus, $F_{y_{cg}}^{B} = F_{z_{cg}}^{B} = 0$ and $F_{x_{cg}}^{B} = -(m_o + m_{BW})g$.

As shown in the prior section, there are control effectiveness parameters for the change in moments due to fundamental wing beat frequency and split-cycle parameters. Equation 57 shows that additionally, there are control derivatives for changes in rolling and pitching moments due to changes in voltage applied to the bob-weight actuator. These expressions will be used in construction of the control effectiveness matrix in the next section.

V. Control Allocation

Form the control effectiveness matrix, whose elements consist of the aerodynamic control derivatives from Table 1 and the bob-weight control derivatives from Equations 57, such that

$$\begin{bmatrix} \Delta \overline{F}_x^B \\ \Delta \overline{F}_y^B \\ \Delta \overline{F}_z^B \\ \Delta \overline{M}_x^B \\ \Delta \overline{M}_y^B \\ \Delta \overline{M}_z^B \end{bmatrix} = \mathbf{B_A} \begin{bmatrix} \delta_{RW} \\ \omega_{RW} \\ \delta_{LW} \\ \omega_{LW} \\ V_{BW} \end{bmatrix} \tag{58}$$

where

$$\mathbf{B_A} \triangleq \begin{bmatrix} 0 & B_{12} & 0 & B_{14} & 0 \\ 0 & 0 & 0 & 0 & 0 \\ -k_D J_1(1)\omega_o & 0 & -k_D J_1(1)\omega_o & 0 & 0 \\ -\frac{1}{2}k_D\omega_o(y_{cp}^{WP}+wJ_1(1)) & 0 & \frac{1}{2}k_D\omega_o(y_{cp}^{WP}+wJ_1(1)) & 0 & B_{45} \\ B_{51} & 0 & B_{53} & 0 & B_{55} \\ 0 & B_{62} & 0 & B_{64} & 0 \end{bmatrix} \tag{59}$$

where $B_{12} = B_{14} = k_L\omega_o$, $B_{62} = -B_{64} = -2k_L\omega_o\left[y_{cp}^{WP}J_1(1) + \frac{w}{4}\right]$,
$B_{51} = J_1(1)\omega_o\left[k_Lx_{cp}^{WP}\cos\alpha + k_D(x_{cp}^{WP}\sin\alpha + \Delta x_R^B)\right]$. Additionally,
$B_{53} = J_1(1)\omega_o\left[k_Lx_{cp}^{WP}\cos\alpha + k_D(x_{cp}^{WP}\sin\alpha + \Delta x_L^B)\right]$, $B_{45} = -k_{BW}\left(\frac{m_{BW}}{m_o+m_{BW}}\right)F_{y_{cg}}^B$ and
$B_{55} = k_{BW}\left(\frac{m_{BW}}{m_o+m_{BW}}\right)F_{x_{cg}}^B$. In order to compute the control vector, a pseudo-inverse solution
to Equation 58 is utilized.

Examination of this matrix reveals what is possible to achieve by manipulating the four
aerodynamic control input parameters and the bob-weight. The rank of this matrix is five.
Most obviously, it is not possible to generate direct side forces on the vehicle using the
five control parameters. The next observation is that rows associated with the z-force and
pitching moment would be linearly dependent for $\Delta z_R^B = \Delta z_L^B = 0$ and $\Delta x_R^B = \Delta x_L^B$ if it
were not for the presence of the bob-weight actuator. These conditions would exist on a well
designed vehicle because of the plane of symmetry, and the fact that from a vehicle design
perspective, it is desirable that the z-offset between the nominal center-of-gravity and the
wing root hinge points be zero. This arrangement eliminates a source of undesirable non-zero
pitching moment associated with ω_o. Such pitching moments would tend to force the vehicle
out of trim and destabilize the hover condition unless active control were applied. The split-
cycle control concept was conceived to provide a set of control inputs that affect the vehicle
forces and moments in one axis at-a-time in order provide a high level of decoupling. The
sparsity of the control effectiveness matrix shows that the concept goes far towards achieving
this desired effect. Notably:

- Symmetric manipulation of the fundamental wing beat frequencies provides x-body
  axis control.

- Manipulation of the split-cycle parameters has no effect upon the x-body axis. Physi-
  cally, this is because the increase in dynamic pressure on one half of the stroke is offset
  by a decrease in dynamic pressure on the other half, resulting in zero net change in
  body force when averaged over a cycle.

- Zero z-body force is achieved when the split-cycle parameters are zero, which is a
  result of drag cancelation on the up and down stroke when the wing-beat cycle is
  temporally symmetric. Non-zero z-body forces are generated when the strokes are
  temporally asymmetric across the wing beat cycle. When the split-cycle parameters
  are varied symmetrically, they can be used to cause the vehicle to translate forwards
  or backwards.

- Rolling moments can be generated by changing the split-cycle parameters and are
  independent of the other control inputs. The split-cycle parameters create a non-zero

cycle averaged drag on each wing due to temporal asymmetry over the wing beat cycle. This non-zero drag acting over a moment arm creates the rolling moment.

- As noted above, pure z-body forces can be generated by symmetric variation of the split-cycle parameters, which does not introduce a rolling moment due to the opposite signs and equal magnitude of the rolling moment split-cycle control derivatives.

- Pitching moments are generated by manipulation of the split-cycle parameters and will be linearly correlated with the z-force used to control fore/aft translation. The pitching moment that is generated tends to tilt the stroke plane in the direction of translation; thereby leading to an increase in fore or aft velocity.

- Yawing moments can be generated by asymmetric variations in the fundamental wing beat frequencies. Symmetric variations cause a change in x-body force; thus, by appropriate control allocation, the x-body force and yawing moment can be decoupled. Furthermore, yawing moment is uncoupled from all other forces and moments, when $\Delta z_R^B = \Delta z_L^B = 0$, which should be the case by design.

Finally, note that the rows associated with the rolling and yawing moments are linearly independent from all other rows, meaning that they can be independently controlled using the four aerodynamic control inputs. In short, with the four aerodynamic controls, the x-body and z-body forces and rolling and yawing moments can be manipulated. For high speed translation longitudinally, a pitch-to-translate strategy can utilized using the bob-weight.

VI.   Control Law Implementation

Utilizing the analysis presented, a simulation of the flapping wing micro air vehicle was developed. Controllers were designed to track altitude, forward translation, roll, pitch, and yaw commands. The choice of a split-cycle frequency modulated control strategy led to a nearly decoupled cycle-averaged control input matrix. Because of the structure of the control input matrix, and the fact that the aircraft near hover is effectively described by a bank of decoupled integrators, it is possible to use simple SISO methods to design feedback control loops for each controllable axis. A block diagram of the control structure is shown in Figure 3. Five axes are actively controlled or regulated: altitude, forward position, roll attitude, pitch attitude, yaw attitude, and their derivatives. Each axis is tuned to achieve a second-order response using a combination of rate and position feedback and reference commands to specify desired accelerations. These acceleration commands are multiplied by the mass (in the case of generating a desired force) or the appropriate moment of inertia term (in the case of generating a desired moment). The SISO controllers are designed as though the

desired forces and moments could be generated as continuous and steady functions of time; however, the physics of the flapping wings dictates that the forces will be periodic functions of time. The matrix $\mathbf{B_A}$ describes the relationship between the cycle-averaged forces and moments and the fundamental frequency, split cycle parameters and bob-weight position. A pseudo-inverse control allocation scheme then determines the necessary control inputs to
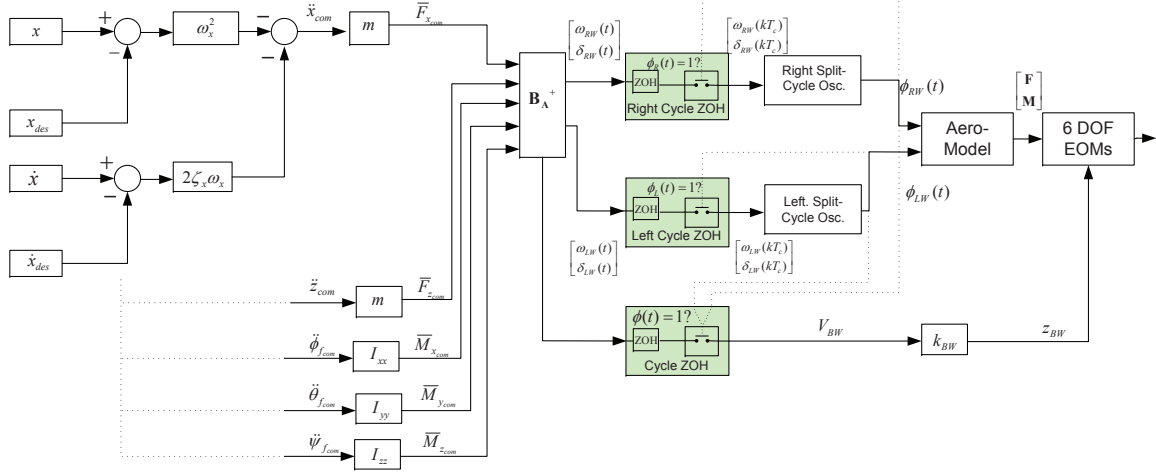

Figure 3. Five degree-of-freedom split-cycle controller.

produce the desired cycle-averaged forces and moments. The control allocator computes the fundamental frequencies and split-cycle parameters based on the instantaneous force and moment commands. The fundamental frequencies and split-cycle parameters govern the behavior of oscillators that generate time varying wing position commands. Inputs to the oscillators are held constant over the course of a wing beat in order to avoid changing the shape of the split-cycle waveform. The logic used to accomplish this function is called a cycle zero-order hold (CZOH). The output of the oscillators are applied to the bimorph piezoelectric actuators and it is assumed that the actuator bandwidth is sufficient to track the wing position commands. The instantaneous aerodynamic forces and moments are computed using a modified blade-element model and applied to the 6 DOF equations-of-motion. The subsequent section shows the results of applying the split-cycle control law to a simulation of an aircraft that is driven by the instantaneous forces and moments produced by the blade-element aerodynamic model.

VII. Results

Utilizing the analysis presented here and in Part I,[1] a simulation of the flapping wing micro air vehicle was produced. Control laws were designed for altitude, forward translation,

rolling, pitching, and yawing moments. Figure 4 shows the three-dimensional trajectory that the vehicle is commanded to follow. The vehicle begins at (0,0,0), rotates to align heading with point 1 and translates to point 1, then performs similar heading alignment and translation to move to points 2, 3, 4, and finally 5. Some of the vehicle properties are shown in Table VII.

Variable	Value	Units
m_o	60	mg
m_{bw}	20	mg
Height	11	mm
Width	4	mm
Depth	1	mm
I_A	1395	mm^4
k_{BW}	0.165e-5	$\frac{m}{Volt}$
Nominal CG Location	$\begin{bmatrix} 5.5 & 0 & 0 \end{bmatrix}$	mm
c_{max}	4	mm
d_b	3	mm
R	15	mm
Δr_R^B	$\begin{bmatrix} 3.5 & 2 & 0 \end{bmatrix}$	mm
Δr_L^B	$\begin{bmatrix} 3.5 & -2 & 0 \end{bmatrix}$	mm
α_U	45	deg
α_D	45	deg
Hover Frequency $= \omega_o = \sqrt{\frac{weight}{.5\rho C_L(\alpha) I_A}}$	113.61	Hz

Table 2. Aerodynamic forces expressed in local spar and body frames.

Figures 5 and 6 shows the commanded and actual positions and attitudes of the vehicle center-of-gravity used to achieve waypoint following. Tracking performance is acceptable and the vehicle is capable of performing the desired maneuvers. Figures 7 shows the left and right wing fundamental and split-cycle frequencies used during this simulation. There are small differences between the fundamental and split-cycle frequencies of the left and right wing. These differences result in a roll for the vehicle and are used to align the vehicle's heading with the next waypoint. The voltage applied to the bob-weight actuator and the location of the vehicle center-of-gravity in the z body-axis direction are shown in Figure 8. The nominal z body-axis center-of-gravity location is 0. Hence, it can be seen that the

center-of-gravity is shifted by a max of about $-0.05\ mm$. This corresponds to a $-0.21\ mm$ shift in the z-position of the bob-weight. The bob-weight was constrained to move no more than $0.25\ mm$ so this is nearly the maximum z direction shift of the center-of-gravity. These results show that the bob-weight is active and is used to generate pitching moments. The trajectory that was chosen for this simulation is acceptable and the vehicle has sufficient control authority to perform the necessary maneuvers.
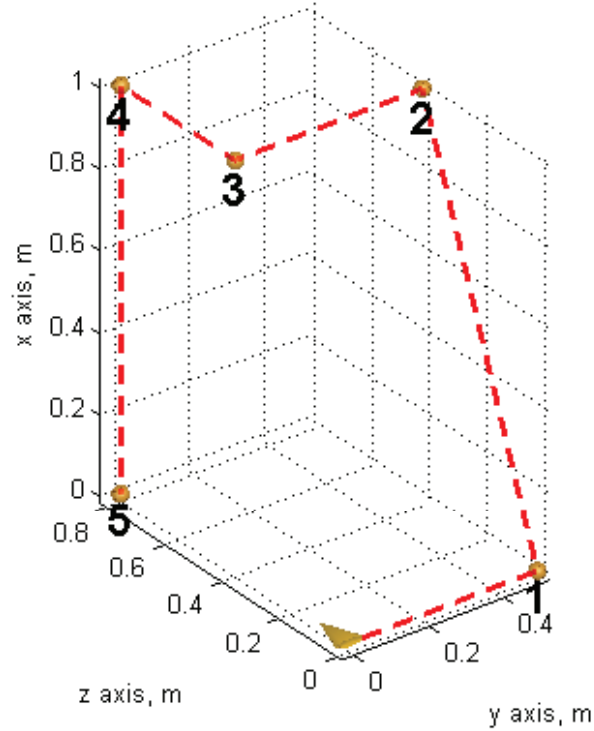

Figure 4. Desired trajectory.

VIII. Summary

This paper has described the split-cycle formulation and has presented a derivation of all split-cycle related parameters. The effects of a bob-weight upon the body-axis forces and moments were computed and then, expressions for the cycle-averaged control derivatives associated with the variations in the fundamental wing beat frequencies, split-cycle parameters, and bob-weight position were developed. The expressions were linearized about a hover flight condition and a control allocation strategy was proposed. Insight into the controllability of this vehicle was provided by interpreting the structure of the control effectiveness matrix. The analysis presented shows that the use of split-cycle constant-period
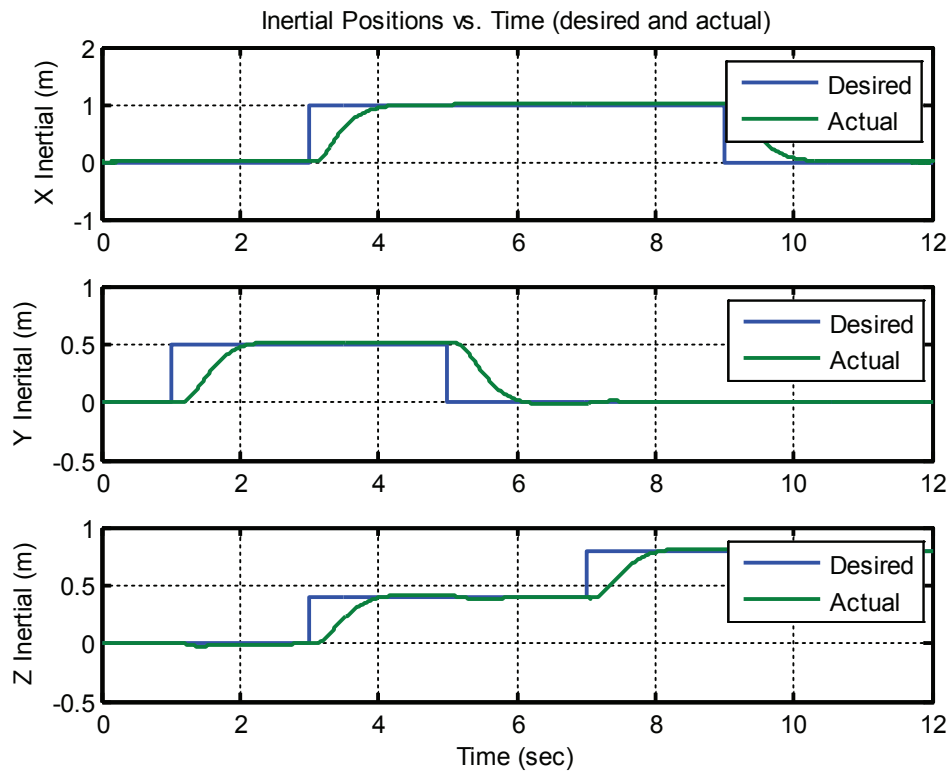
Figure 5. Inertial positions.

frequency modulation, with independently actuated wings, allows one to manipulate the x-body and z-body axis forces. The y-body force is not directly controllable using the split-cycle approach as presented. Direct manipulation of the y-body force, given the physical design constraints of the proposed vehicle, would require that the frequency of the oscillators driving the wings be varied more than once per cycle. Rolling and yawing moments can also be independently varied using the split-cycle technique. A pitching moment can also be generated; however, it cannot be generated independently of the z-body force or the rolling moment. Thus, a bob-weight was introduced to cancel these undesirable changes in the pitching moment when manipulating the split-cycle parameters to generate z-body forces and rolling moments. Given the ability to independently manipulate 5 out of the 6 cycle-averaged body-axis forces and moments, untethered controlled flight with insect-like maneuverability appears to be feasible.

References

[1]Doman, D. B., Oppenheimer, M. W., and Sigthorsson, D. O., "Dynamics and Control of a Minimally Actuated Biomimetic Vehicle: Part I - Aerodynamic Model," Submitted to 2009 AIAA Guidance, Navigation and Control Conference, Aug. 2009.
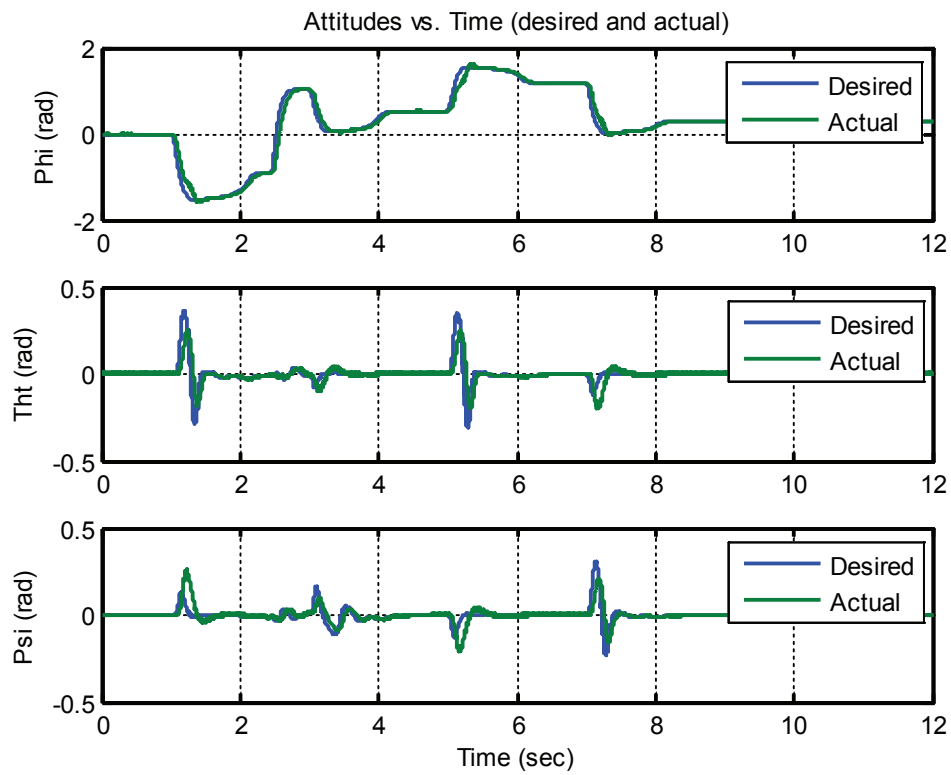
Figure 6. Attitudes.

[2]Wood, R. J., "The First Takeoff of a Biologically Inspired At-Scale Robotic Insect," *IEEE Transactions on Robotics*, Vol. 24, No. 2, 2007, pp. 341–347.

[3]Doman, D. and Ngo, A., "Dynamic Inversion-Based Adaptive/Reconfigurable Control of the X-33 on Ascent," *Journal of Guidance, Control, and Dynamics*, Vol. 25, No. 2, 2002, pp. 275–284.
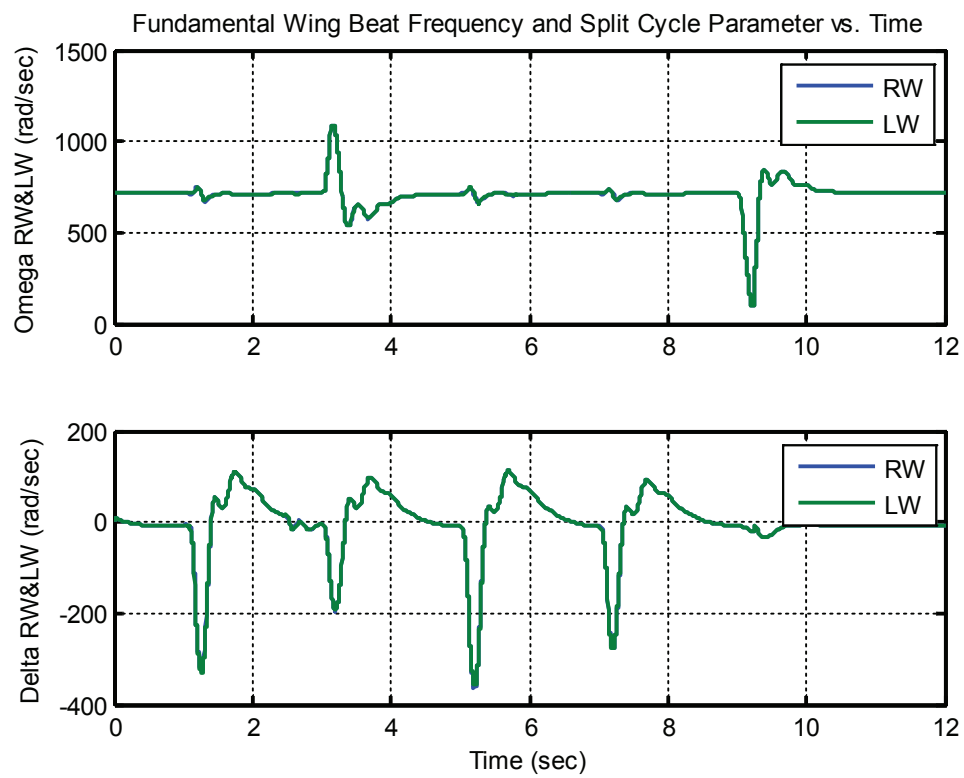
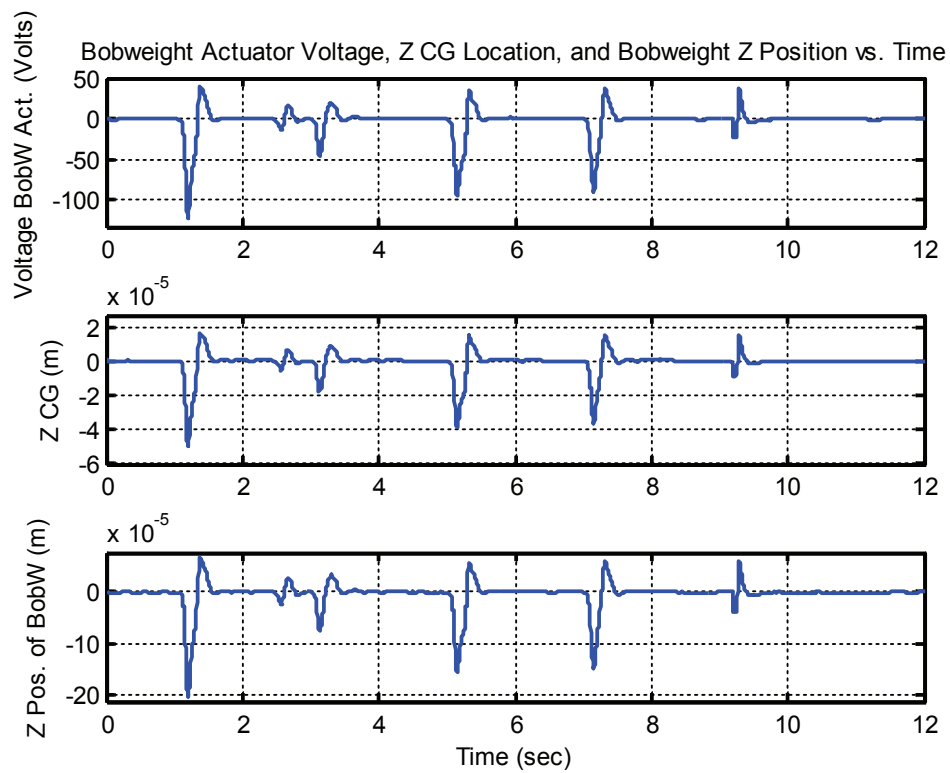Figure 7. Fundamental and split-cycle frequencies.

Figure 8. Voltage applied to bob-weight actuator and center-of-gravity shift in z direction due to bob-weight movement.